TU-874

Measurements of neutral vector resonance in Higgsless models at the LHC

Masaki Asano[a] and Yasuhiro Shimizu[a,b]

[a] *Department of Physics, Tohoku University, Sendai 980-8578, Japan*
[b] *IIAIR, Tohoku University, Sendai 980-8578, Japan*

Abstract

In Higgsless models, new vector resonances appear to restore the unitarity of the W_LW_L scattering amplitude without the Higgs boson. In the ideal delocalized three site Higgsless model, one of large production cross section of the neutral vector resonance (Z') at the Large Hadron Collider is the W-associated production, $pp \to Z'W^\pm \to W^\mp W^\pm W^\pm$. Although the dileptonic decay channel, $l\nu l'\nu' jj$, is experimentally clean to search for the Z' signals, it is difficult to reconstruct the Z' invariant mass due to the two neutrinos in the final state. We study collider signatures of Z' using the M_{T2}-Assisted On-Shell (MAOS) reconstruction of the missing neutrino momenta. We show the prospect of the Z' mass determination in the channel, $l\nu l'\nu' jj$, at the Large Hadron Collider.

1 Introduction

The Large Hadron Collider (LHC) experiments are now operating. At the LHC, a new electroweak signal will be discovered because the unitarity of the W_LW_L scattering amplitude is violated at the scale higher around 1 TeV due to the E^2 dependence. One of the candidates is a signal from a scalar $SU(2)_L$ doublet, called the Higgs boson. Due to the contribution from the Higgs boson, the E^2 dependence of the W_LW_L scattering amplitude vanishes in the standard model (SM).

On the other hand, it is also possible to maintain the unitarity without the Higgs scalar in Higgsless models [1, 2]. In Higgsless models, vector resonances which are responsible for the restoration of the unitarity of the W_LW_L scattering amplitude will be produced at the LHC. The masses are less than around 1 TeV to avoid the unitarity violation, but such particles are strictly constrained by direct observation if their couplings to SM fermions are similar to the SM ones [3]. Also the coupling induces a large correction to electroweak precision measurements at the tree level. To avoid the constraints, the couplings should be suppressed and it is realized by the fermion delocalization [4, 5, 6, 7, 8, 9]. The vector resonances therefore have only small coupling to the SM fermions in Higgsless models.

Fermiophobic vector resonances can be produced mainly by the weak gauge boson associated process or the vector boson fusion process and mainly decay into the weak gauge bosons at the LHC. The measurements of charged vector resonance have been studied [10, 11, 12, 13, 14]. However, in a case that the W-associated production is dominant, the mass determination of the neutral vector resonance (Z') is very difficult because there are three W bosons in the final state. A way using $W^{\pm}W^{\pm}W^{\mp} \to l^{\pm}\nu l'^{\pm}\nu' jj$ mode is proposed by Tao Han et.al.[14], and they showed that the mass can be read off by an endpoint of the $m(ljj)$ distribution from the parton level study.

In this paper, we show that neutral vector resonance can be reconstructed even in $WWW \to l\nu l'\nu' jj$ final state using M_{T2} Assisted On-Shell (MAOS) reconstruction of missing momenta [15, 16, 17]. Since MAOS momenta equal true neutrino four momenta at the M_{T2} [18] endpoint of $WW \to l\nu l'\nu'$ system, the Z' mass will be determined by the peak of the invariant mass of reconstructed $W^{\pm}W^{\mp}$ bosons.

This article is organized as follows. In the next section, we briefly review the Higgsless models. In our study, we focus on the three site Higgsless model [19] as a benchmark model. In section 3, we briefly review the MAOS momenta. The Monte Carlo simulation study for measurements of neutral vector resonance at the LHC are discussed in section 4, where we

show the mass will be measured with an integrated luminosity of 100 fb^{-1} at $\sqrt{s} = 14$TeV. Section 5 is devoted to summary and discussion.

2 Higgsless models

In continuum five-dimensional gauge theory, the cancellations of E^2 and E^4 dependence of $W_L W_L$ scattering amplitude are guaranteed by following sum rules [1, 20]:

$$\begin{aligned} \sum_{i=1}^{\infty} g_{Z_i WW}^2 &= g_{WWWW} - g_{ZWW}^2 - g_{\gamma WW}^2, \\ 3\sum_{i=1}^{\infty} g_{Z_i WW}^2 M_{Z_i}^2 &= 4 g_{WWWW} M_W^2 - 3 g_{ZWW}^2 M_Z^2, \end{aligned} \tag{1}$$

where g_{WWWW}, g_{ZWW} and $g_{\gamma WW}$ are the SM $WWWW$, WWZ and γWW coupling constants, respectively. The Z_i represents the i-th KK excitation and Z_1 is also denoted Z' in this paper. The Z' mass should be less than the unitarity violation scale $\sqrt{8\pi}v \sim 1.2$ TeV if there is no Higgs boson nor other vector resonances.

In this paper, we study the collider signatures of the three site Higgsless model [19] as a benchmark model of Higgsless models. The model contains many essential ingredients of Higgsless models and a gauge invariant four-dimensional effective theory of Higgsless models. We briefly review the three site Higgsless model.

The three site Higgsless model is a deconstructed Higgsless model with only three sites *. The model is based on two nonlinear $(SU(2) \times SU(2))/SU(2)$ sigma models. The non-linear sigma fields, U_1 and U_2, are given as

$$U_i = e^{i\pi_i^a \tau^a / f_i} \quad \text{for } i = 1, 2, \tag{2}$$

where π_i^a are Nambu-Goldstone bosons and τ^a are the Pauli matrices. The model incorporates $SU(2) \times SU(2) \times U(1)$ gauge symmetry with gauge coupling strengths g_0, g_1 and g_2, respectively. The vacuum expectation values (VEVs) f_1 and f_2 break the $SU(2) \times SU(2) \times U(1)$

* The gauge sector is equivalent to the Breaking Electroweak Symmetry Strongly (BESS) model [21, 22] one.

Particles	$SU(2)_0$	$SU(2)_1$	$U(1)_2$
q_{L0}, l_{L0}	**2**	**1**	1/6, −1/2
q_{L1}, l_{L1}	**1**	**2**	1/6, −1/2
q_{R1}, l_{R1}	**1**	**2**	1/6, −1/2
u_{R2}, d_{R2}, e_{R2}	**1**	**1**	2/3, −1/3, −1

Table 1: Quantum numbers of fermion fields.

gauge symmetry to $U(1)_{em}$:

$$\begin{aligned}
\mathcal{L}_{gauge} &= \sum_{i=1}^{2} \frac{f_i^2}{4} \mathrm{Tr}\left[(D_\mu U_i)^\dagger (D^\mu U_i)\right] - \sum_{i=0}^{2} \frac{1}{2} \mathrm{Tr}\left[\mathbf{V}_{i\mu\nu}\mathbf{V}_i^{\mu\nu}\right], \qquad (3)\\
D_\mu U_i &\equiv \partial_\mu U_i + i g_{(i-1)} \mathbf{V}_{(i-1)\mu} U_i - i g_i U_i \mathbf{V}_{i\mu}, \qquad \mathbf{V}_{i\mu} = \sum_{a=1,2,3} \frac{\tau^a}{2} V_{i\mu}^a \quad \text{for } i = 0, 1,\\
\mathbf{V}_{i\mu\nu} &\equiv \partial_\mu \mathbf{V}_{i\nu} - \partial_\nu \mathbf{V}_{i\mu} + i g_i \left[\mathbf{V}_{i\mu}, \mathbf{V}_{i\nu}\right], \qquad \mathbf{V}_{2\mu} = \frac{\tau^3}{2} V_{2\mu}^3,
\end{aligned}$$

where the $V_{0(1)}^a$ is the gauge field for the $SU(2)$ gauge group at the site 0(1) and V_2^3 is the gauge field for the $U(1)$ gauge group at the site 2 which is embedded as the τ_3 generator of $SU(2)$. Therefore, this model contains charged and neutral gauge bosons, W' and Z', in addition to the SM W, Z and photon. The combinations of $V_{0,1}^{1,2}$ correspond to the W' and W. On the other hand, the combination of $V_{0,1,2}^3$ are the Z', Z and photon, respectively. For simplicity, we take $f_1 = f_2 = \sqrt{2}v$ in this study.

The left-handed fermions ψ_{L0} and ψ_{L1} are $SU(2)$ doublets coupling to the groups at the sites 0 and 1, respectively. On the other hand, the right handed fermions ψ_{R1} are SU(2) doublets coupling to the group at site 1 and u_{R2}, d_{R2} and e_{R2} are singlets coupling to the group at site 2. The quantum numbers of the fermions are shown in Table 1. The Yukawa couplings are written by

$$\begin{aligned}
\mathcal{L}_{Yukawa} &= \lambda f_1 \bar{\psi}_{L0} U_1 \psi_{R1} + f_2 \bar{\psi}_{L1} U_2 \begin{pmatrix} \lambda'_u & 0 \\ 0 & \lambda'_d \end{pmatrix} \begin{pmatrix} u_{R2} \\ d_{R2} \end{pmatrix} + M \bar{\psi}_{L1} \psi_{R1} + \text{h.c.} \qquad (4)\\
&= \begin{pmatrix} \bar{\psi}_{L0} & \bar{\psi}_{L1} \end{pmatrix} M \begin{pmatrix} \varepsilon_L & 0 \\ 1 & \varepsilon_{uR,dR} \end{pmatrix} \begin{pmatrix} \psi_{R1} \\ u_{R2}, d_{R2} \end{pmatrix} + \text{h.c.},
\end{aligned}$$

where $M\varepsilon_L = \lambda f_1 \equiv m$ and $M\varepsilon_{uR,dR} = \lambda'_{u,d} f_2 \equiv m'_{u,d}$. In this paper, we assume that the m and M are universal for the generation and quark-lepton.

In the limit, $g_0/g_1 \ll 1$ and $g_2/g_1 \ll 1$, the gauge boson masses are given by

$$\begin{aligned}
M_W &\sim \frac{g_0^2}{4} v^2 \left[1 - \frac{1}{4}\left(\frac{g_0}{g_1}\right)^2\right], \quad M_{W'} \sim g_1^2 v^2 \left[1 + \frac{1}{4}\left(\frac{g_0}{g_1}\right)^2\right], \qquad (5)\\
M_Z &\sim \frac{g_0^2}{4c^2} v^2 \left[1 - \frac{(c^2 - s^2)^2}{4c^2}\left(\frac{g_0}{g_1}\right)^2\right], \quad M_{Z'} \sim g_1^2 v^2 \left[1 + \frac{1}{4c^2}\left(\frac{g_0}{g_1}\right)^2\right].
\end{aligned}$$

Here $s = \sin\theta$, $c = \cos\theta$, and $\tan\theta = g_2/g_0$. In the $\varepsilon_L \ll 1$ limit, fermion masses are written as the following:

$$m_{t,b} \sim \frac{m m'_{t,b}}{\sqrt{M^2 + m'^2_{t,b}}}, \quad M_{T,B} \sim \sqrt{M^2 + m'^2_{t,b}}, \tag{6}$$

where we show the masses of the third-generation quarks as an example. The $M_T(M_B)$ is the new heavy top(bottom) quark mass.

The couplings between the light fermions and the heavy gauge bosons are constrained by direct heavy gauge boson search and the electroweak precision measurements. The coupling can be small by delocalizing fermion and ε_L is a parameter which denotes the degree of the delocalization. In the case, $\varepsilon_L = (1+\varepsilon_{fR}^2)^2\{(g_0/g_1)^2/2 + \mathcal{O}((g_0/g_1)^4) + \cdots\}$, the coupling constants are given by

$$g_{ffW'} = 0. \tag{7}$$

This case is called ideal delocalization in which the precision electroweak corrections are minimized at tree level [8] †. In the ideal delocalization case, the lower bound of W' mass, 380 GeV, is given by the bound on the triple gauge vertex from the LEP-II experiments [19].

3 MAOS momentum

In this section, we briefly review the MAOS momentum [15, 16, 17]. The MAOS momentum is defined using the M_{T2} formula [18]. In the $WW \to l(p)\nu(k)l'(p')\nu'(k')$ system, the M_{T2} valuable is written by

$$M_{T2}^2 = \min_{\mathbf{k}_T + \mathbf{k}'_T = \not{\mathbf{p}}_T} \left[\max\left\{M_T^2(\mathbf{p}_T, \mathbf{k}_T), M_T^2(\mathbf{p}'_T, \mathbf{k}'_T)\right\}\right], \tag{8}$$

where $\not{\mathbf{p}}_T$ is the missing transverse momentum and the transverse mass, M_T, is defined by

$$M_T^2(\mathbf{p}_T, \mathbf{k}_T) = 2\left(|\mathbf{p}_T||\mathbf{k}_T| - \mathbf{p}_T \cdot \mathbf{k}_T\right), \tag{9}$$

where the lepton masses are neglected.

The MAOS momenta, k^{MAOS} and k'^{MAOS}, are defined by the following. Assuming $\not{\mathbf{p}}'_T = -(\mathbf{p}_T + \mathbf{p}'_T)$, the transverse momenta of k^{MAOS} and k'^{MAOS} are defined by

$$\mathbf{k}_T^{MAOS} = -\mathbf{p}'_T, \quad \mathbf{k}_T'^{MAOS} = -\mathbf{p}_T, \tag{10}$$

† At the 1-loop level, the parameter does not satisfy the electroweak precision measurements [23]. But we take the parameter in the following analysis since the correction to the signal in our collider study is small even if we take a parameter which satisfies the electroweak precision measurements at the 1-loop level.

$m_{Z'}$ [GeV]	$m_{W'}$ [GeV]	M [GeV]	$\lvert g_{Z'WW}\rvert$	$\sigma(Z'W)$ [fb]	$\sigma(Z'qq)$ [fb]	Br($Z' \to WW$)
380	378	4000	0.071	593	144	97%
500	498	4000	0.054	178	42	99%

Table 2: Representative points in this study. The $\sigma(Z'W)$ and $\sigma(Z'qq)$ are the $pp \to Z'W$ production cross section and $pp \to Z'qq$ production cross section, respectively.

and

$$\begin{aligned} M_{T2}(\mathbf{p}_T, \mathbf{p}'_T, \not{\mathbf{p}}_T) &= \sqrt{2}\sqrt{\left(|\mathbf{p}_T||\mathbf{k}_T^{MAOS}| - \mathbf{p}_T \cdot \mathbf{k}_T^{MAOS}\right)}, \\ &= \sqrt{2}\sqrt{\left(|\mathbf{p}'_T||\mathbf{k}'^{MAOS}_T| - \mathbf{p}'_T \cdot \mathbf{k}'^{MAOS}_T\right)}. \end{aligned} \tag{11}$$

The MAOS momenta are also required to satisfy the following conditions in the $WW \to l(p)\nu(k)l'(p')\nu'(k')$ system:

$$\begin{aligned} \left(k^{MAOS}\right)^2 &= \left(k'^{MAOS}\right)^2 = 0, \\ \left(p + k^{MAOS}\right)^2 &= \left(p' + k'^{MAOS}\right)^2 = M_{T2}^2. \end{aligned} \tag{12}$$

From these equations, the longitudinal momenta of k^{MAOS} and k'^{MAOS} are also determined by

$$k_L^{MAOS}(\pm) = \frac{|\mathbf{k}_T^{MAOS}|}{|\mathbf{p}_T|} p_L, \quad k'^{MAOS}_L(\pm) = \frac{|\mathbf{k}'^{MAOS}_T|}{|\mathbf{p}'_T|} p'_L. \tag{13}$$

At the M_{T2} endpoint, the MAOS momenta become equal to the final state neutrino momenta k, k', respectively.

In the next section, we show that the fermiophobic Z' can be reconstructed using MAOS momenta of neutrinos at the LHC through Monte Carlo simulations. The Z' mass can be measured by the invariant mass peak of the reconstructed WW.

4 Monte Carlo Simulation

We study the possibility of Z' reconstruction through Monte Carlo simulations in this section. We investigate the ideal delocalized three site Higgsless model as a benchmark model and the parameters at the representative points are summarized in Table 2. For the Monte Carlo simulation, we have produced the signal parton events by Madgraph/Madevent [24, 25] and they have been hadronized by PYTHIA [26]. For the SM backgrounds, we have generated the events using ALPGEN [27] and HERWIG [28, 29]. Our detector simulation is based on ACERDET [30]. Hereafter we assume an integrated luminosity of $\mathcal{L} = 100$ fb^{-1}.

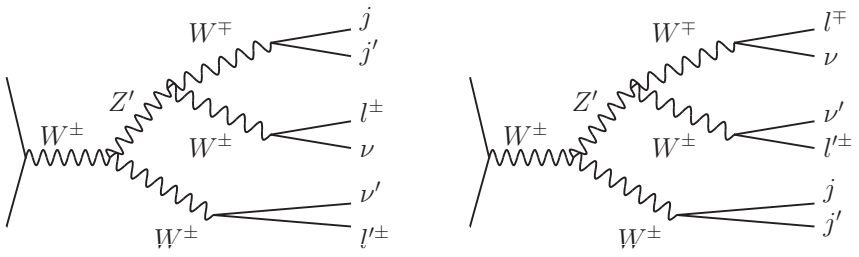

Figure 1: (Left) Feynman diagram for the same sign dilepton mode. (Right) Feynman diagram for the opposite sign dilepton mode.

In our analysis, we concentrate on the W-associated production depicted in Fig. 1, especially in the following dilepton mode,

$$pp \to W^\pm Z' \to \begin{cases} W^\pm\ (W^+W^-) \to (l^\pm\nu)((l^\pm\nu)(jj)) & \text{(same sign)}, \\ W^\pm\ (W^+W^-) \to (jj)((l^\pm\nu)(l^\mp\nu)) & \text{(opposite sign)}, \end{cases} \tag{14}$$

because the large SM backgrounds can be reduced in the dilepton modes. In particular, it is shown that the $t\bar{t}$ background is significantly reduced for the same sign dilepton mode [14].

In the signal mode, there are three W bosons; two W bosons decay leptonically and one W decays hadronically. In order to reconstruct the hadronically decaying W, we require the following cuts:

- at least two and less than three hard jets with $p_T > 20$ GeV,
- 65 GeV $< m_{jj} <$ 95 GeV,

where the m_{jj} is the invariant mass of two hard jets. We also impose b-jet veto to reduce $t\bar{t}$ events.

To reconstruct the two W bosons which decay leptonically, we use neutrino MAOS momenta which are defined by a M_{T2} valuable using two leptons and missing momenta. In the same (opposite) sign charge mode, we require the following:

- two leptons with the same (opposite) charge with $p_T > 10$ GeV,
- $\not{p}_T > 50$ GeV.

In the same sign dilepton mode, the requirement of the same charge lepton reduce the $t\bar{t}$ events significantly. On the other hand, huge $t\bar{t}$ events still remain for the opposite sign

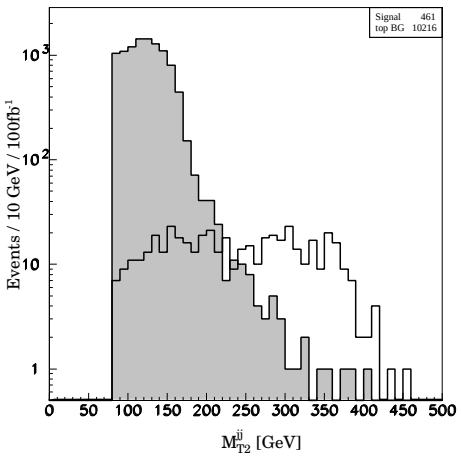

Figure 2: The M_{T2}^{jj} distribution in the opposite sign dilepton mode for $m_{Z'} = 380$ GeV (white) and the $t\bar{t}$ backgrounds (hatched). Here the integrated luminosity is 100 fb^{-1} and the mass of the missing particle is set to m_W.

dilepton mode. To reduce the $t\bar{t}$ events, we also define another M_{T2} valuable, M_{T2}^{jj}, in which we define the "effective missing p_T", $\not{\mathbf{p}}_T^{\rm eff} = \not{\mathbf{p}}_T + \mathbf{p}_{Tl1} + \mathbf{p}_{Tl2}$ and the mass of missing particle, $m_X = m_W$, in the opposite charge mode. The M_{T2}^{jj} valuable should have a maximum value at the top quark mass taking the missing particle mass, $m_X = m_W$, because we deal with two W bosons decaying leptonically as missing particles. In Fig. 2, we show the $M_{T2}^{jj}(m_X = m_W)$ distributions for the signal with $m_{Z'} = 380$ GeV and the $t\bar{t}$ events after the jet and lepton cuts. We can see a sharp endpoint around the top quark mass for the $t\bar{t}$ events while the signal events give larger M_{T2}^{jj}. Therefore, we impose $M_{T2}^{jj}(m_X = m_W) > 200$ GeV to cut the $t\bar{t}$ events. The procedure reduces the combinatorial ambiguity of the jets and the leptons than a procedure using M_{T2}^{jljl} which should have a maximum value at the top quark mass taking the missing particle mass, $m_X = 0$ GeV.

In addition, we also impose other cuts, the value of $M_{\rm eff}$, which is defined as a scalar sum of the visible and the missing momenta [31], and invariant mass of two leptons, m_{ll}, listed in Table 3. The m_{ll} cuts reduce the Z boson and $t\bar{t}$ backgrounds because a lepton from a top quark decay is softer than a lepton in the signal events. In Table 4 (5), we show the number of events after the selection cuts for the same (opposite) sign mode.

From the MAOS momenta, we can reconstruct the invariant mass of the Z' as follows:

$$m_{Z'}^2 = \begin{cases} (p + k^{MAOS} + p_{j_1} + p_{j_2})^2 & \text{(same sign)}, \\ (p + k^{MAOS} + p' + k'^{MAOS})^2 & \text{(opposite sign)}. \end{cases} \tag{15}$$

In both modes, there is a two-fold ambiguity to reconstruct the Z' invariant mass from two

	$m_{Z'} = 380$ GeV	$m_{Z'} = 500$ GeV
same	$M_{\rm eff} > 500$ GeV and $m_{ll} > 130$ GeV	$M_{\rm eff} > 500$ GeV and $m_{ll} > 130$ GeV
opposite	$M_{\rm eff} > 600$ GeV and $m_{ll} > 110$ GeV	$M_{\rm eff} > 700$ GeV and $m_{ll} > 110$ GeV

Table 3: Cuts used in the analysis for the same and the opposite sign lepton modes.

W bosons. In the same sign mode, there are two choices to combine the lepton momenta with the hadron momenta. We choose the combination which gives the smaller $m_{Z'}$ in our analysis. On the other hand, we reconstruct Z' invariant mass from two W bosons which decay leptonically in order to confirm the charge of the Z' in the opposite sign mode.

In Figs. 3 and 4, we show the invariant mass distributions of Z' in the same and opposite sign dilepton mode for $m_{Z'} = 380$ GeV, respectively. The hatched histograms are the SM backgrounds. Although the MAOS momenta become equal to the true neutrino momenta only at the M_{T2} endpoint, $M_{T2} \simeq 80$ GeV, we use the MAOS momenta in wide M_{T2} regions and plot the invariant mass distributions of Z' for $M_{T2} > 60, 40, 20, 0$ GeV. [‡] In Fig. 3 we can see the peaks around the true Z' mass regions for all the cases. The shape becomes sharper when we use the MAOS momenta in the higher M_{T2} regions. However, the number of the events becomes smaller. Thanks to the M_{T2}^{jj} cut, we can see clear signal peaks around the true $m_{Z'}$ value even in the opposite sign mode. Although the shapes of the invariant distributions are slightly irregular compared with the same sign mode, we can determine the Z' mass from the peak.

In Figs. 5 and 6, we show the invariant mass distributions of Z' in the same and opposite sign dilepton mode for $m_{Z'} = 500$ GeV, respectively. Since the production cross section is smaller compared with the $m_{Z'} = 380$ GeV case, the numbers of events are limited if we use the tight M_{T2} cut. In the opposite sign mode, we cannot see clear peaks for the $M_{T2} > 20, 40, 60$ GeV cases. However, we can see the peaks around the true $m_{Z'}$ region even for $m_{Z'} = 500$ GeV in the both modes.

5 Summary and Discussion

In this paper, we have studied the search for the neutral vector resonance, focusing on a fermiophobic case at the LHC. Such fermiophobic vector bosons are predicted by perturbative TeV scale scenarios without the Higgs boson, and can be produced in the W-

[‡] When the Z' is heavy enough to decay to two on-shell W bosons, there is the other definition of the MAOS momenta [15]. Even if we take the MAOS momenta, the distributions are not drastically changed in our study with 100 fb^{-1}.

	Selection cut	Signal (380, 500 GeV)	top BG	W boson BG
jet	# of jets ($P_T > 20$ GeV)=2	(4844, 1451)	774624	5862
	65 GeV $< m_{jj} <$ 95 GeV	(1116, 313)	124142	1485
	b veto	(1069, 299)	44009	1410
lepton	2 same charge leptons ($P_T > 10$ GeV)	(284, 96)	1234	91
	$\not{p}_T > 50$ GeV	(257, 90)	777	64
other	$M_{\rm eff} > 500$ GeV	(207, 85)	21	9
	$m_{ll} > 130$ GeV	(167, 74)	0	5

Table 4: Number of events after selection cuts for the same sign mode with an integrated luminosity $\mathcal{L} = 100^{-1}$ fb.

	Selection cut	Signal (380, 500 GeV)	top BG	W boson BG
jet	# of jets ($P_T > 20$ GeV)=2	(4844, 1451)	774624	5862
	65 GeV $< m_{jj} <$ 95 GeV	(1116, 313)	124142	1485
	b veto	(1069, 299)	44009	1410
lepton	2 opposite charge leptons ($P_T > 10$ GeV)	(508, 141)	15845	993
	$\not{p}_T > 50$ GeV	(461, 130)	10216	533
M_{T2}^{jj}	M_{T2}^{jj}	(289, 99)	125	44
other	$M_{\rm eff} > (600, 700)$ GeV	(254, 83)	(25, 9)	(16, 12)
	$m_{ll} > 110$ GeV	(206, 67)	(9, 1)	(11, 8)

Table 5: Number of events after selection cuts for the opposite sign mode with an integrated luminosity $\mathcal{L} = 100^{-1}$ fb.

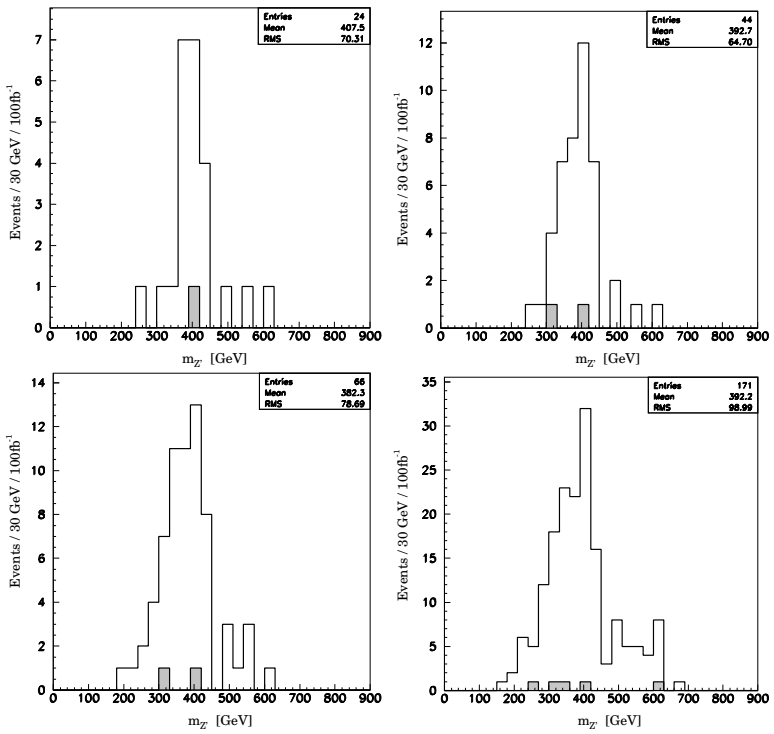

Figure 3: The invariant mass distributions of Z' in the same sign dilepton mode for $m_{Z'} = 380$ GeV with an integrated luminosity $\mathcal{L} = 100^{-1}$ fb. Here we impose the cuts listed in Table 4 and $M_{T2} > 60$(top left), 40(top right), 20(bottom left), 0(bottom right) GeV. The hatched histograms are the SM backgrounds.

associated processes at the LHC. We have studied the dilepton decay modes, $pp \to W^{\pm}Z' \to W^{\pm}W^{\pm}W^{\mp} \to l\nu l'\nu' jj$, since the SM model backgrounds are suppressed. There are two neutrinos in the dilepton modes and we cannot measure each neutrino momentum directly. In order to determine the neutrino momenta we use the MAOS momenta. From the MAOS momenta we can reconstruct the invariant mass of the neutral vector boson and the mass of the neutral vector resonance can be determined by the peak of the invariant mass distribution.

We have applied the method to both the same and the opposite sign dilepton modes. We have found that the M_{T2}^{jj} cut is very effective to reduce the $t\bar{t}$ background, especially in the opposite sign mode. We can obtain clear invariant mass distributions of the vector resonance and the shape of the invariant mass distributions changes depending on the M_{T2} cut. Although the shape becomes broader if we use a looser M_{T2} cut, we have found that the peak positions of the invariant mass distributions do not change drastically. To measure the mass more accurately, we should optimize the M_{T2} cut analysing detailed Monte Carlo simulations.

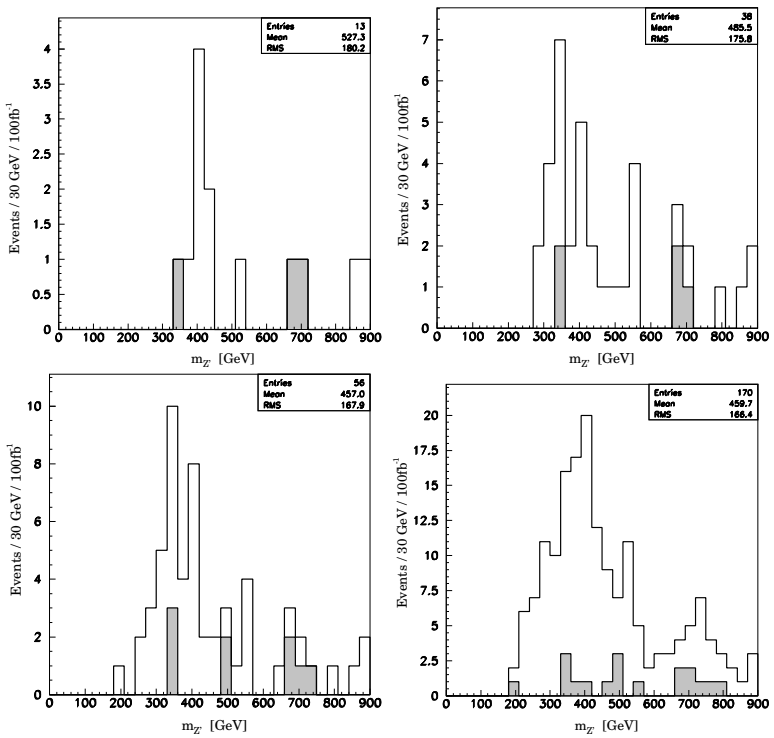

Figure 4: The invariant mass distributions in the opposite sign dilepton mode for $m_{Z'} = 380$ GeV with an integrated luminosity $\mathcal{L} = 100^{-1}$ fb. Here we impose the cuts listed in Table 5 and $M_{T2} > 60$(top left), 40(top right), 20(bottom left), 0(bottom right) GeV. The hatched histograms are the SM backgrounds.

Let us discuss advantages of our method compared to other analyses on the Z' measurements at the LHC. Since we have studied the dilepton mode in the Z' decay, the SM backgrounds are reduced and we can see the clear peak of the Z' resonance. From the charge of the dileptons, we can confirm the charge of the resonance in the opposite sign mode. In the same sign mode, we can also infer that the charge is neutral unless double charged particles exist. If we consider one lepton mode, $Z'W \to l\nu jjjj$ or $Z' \to W^+W^- \to l\nu jj$, which is produced via the vector boson fusion or Drell-Yan production process, the Z' and W' resonances may overlap each other due to difficulty of the $W(Z)$ identification at the LHC. However, it is possible to study the Z' peak separately in our method. In the three site Higgsless model, the Z' can also be measured via Drell-Yan production process in the semileptonic decay mode because the couplings with SM fermions are not zero even if we take the ideal delocalization [32, 33, 34]. Using MAOS momenta, the Z' may also be measured in the leptonic decay mode, $Z' \to WW \to l\nu l'\nu'$, without W' contamination. The similar signal, Higgs $\to WW \to l\nu l'\nu'$, has been studied by using MAOS momenta [16, 17]. Combining the

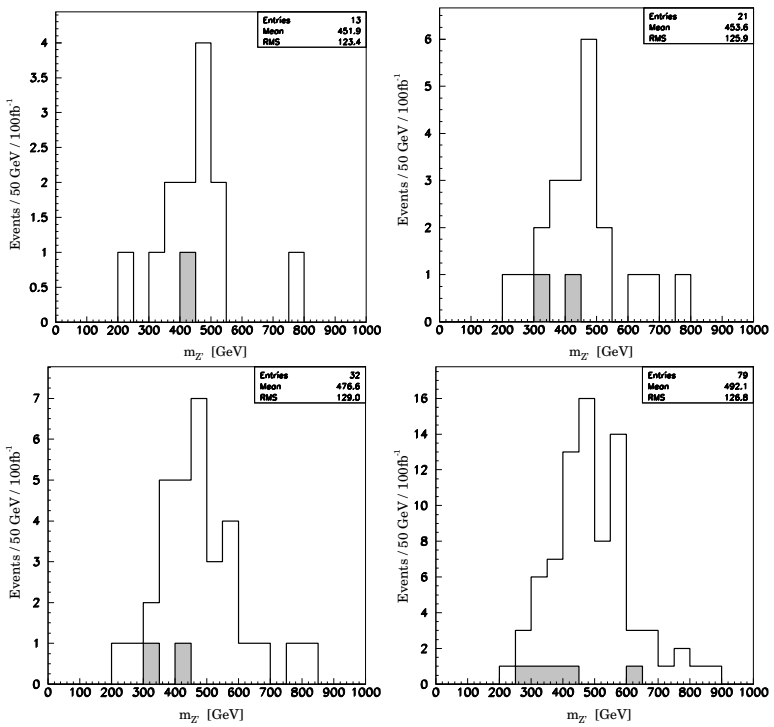

Figure 5: The invariant mass distributions in the same sign dilepton mode for $m_{Z'} = 500$ GeV with an integrated luminosity $\mathcal{L} = 100^{-1}$ fb. Here we impose the cuts listed in Table 4 and $M_{T2} > 60$(top left), 40(top right), 20(bottom left), 0(bottom right) GeV. The hatched histograms are the SM backgrounds.

results from the W-associated and Drell-Yan production process study with MAOS momenta, we may also determine the Z' couplings with weak gauge bosons and SM fermions.

Although we focus on the Z' measurement in the three-site Higgsless model in this paper, the method will be also useful for the mass measurement of general fermiophobic neutral vector resonances.

Acknowledgments

We would like to thank Masafumi Kurachi for discussions and comments. This work is supported in part by the Grant-in-Aid for the Global COE Program Weaving Science Web beyond Particle-matter Hierarchy from the Ministry of Education, Culture, Sports, Science and Technology of Japan (M. A.).

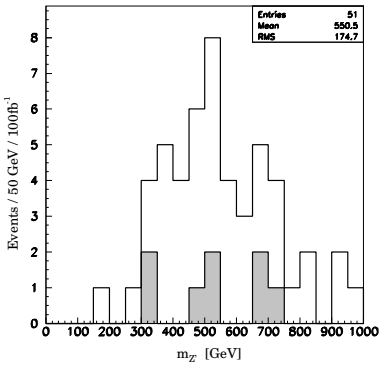

Figure 6: The invariant mass distributions in the opposite sign dilepton mode for $m_{Z'} = 500$ GeV with an integrated luminosity $\mathcal{L} = 100^{-1}$ fb. Here we take the cuts listed in Table 5 and $M_{T2} > 0$ GeV. The hatched histograms are the SM backgrounds.

References

[1] C. Csaki, C. Grojean, H. Murayama, L. Pilo and J. Terning, Phys. Rev. D **69** (2004) 055006 [arXiv:hep-ph/0305237].

[2] C. Csaki, C. Grojean, L. Pilo and J. Terning, Phys. Rev. Lett. **92** (2004) 101802 [arXiv:hep-ph/0308038].

[3] C. Amsler *et al.* [Particle Data Group], Phys. Lett. B **667** (2008) 1.

[4] G. Cacciapaglia, C. Csaki, C. Grojean and J. Terning, Phys. Rev. D **71** (2005) 035015 [arXiv:hep-ph/0409126].

[5] R. Foadi, S. Gopalakrishna and C. Schmidt, Phys. Lett. B **606** (2005) 157 [arXiv:hep-ph/0409266].

[6] R. S. Chivukula, E. H. Simmons, H. J. He, M. Kurachi and M. Tanabashi, Phys. Rev. D **71** (2005) 115001 [arXiv:hep-ph/0502162].

[7] R. Casalbuoni, S. De Curtis, D. Dolce and D. Dominici, Phys. Rev. D **71** (2005) 075015 [arXiv:hep-ph/0502209].

[8] R. S. Chivukula, E. H. Simmons, H. J. He, M. Kurachi and M. Tanabashi, Phys. Rev. D **72** (2005) 015008 [arXiv:hep-ph/0504114].

[9] R. S. Chivukula, E. H. Simmons, H. J. He, M. Kurachi and M. Tanabashi, Phys. Rev. D **72** (2005) 095013 [arXiv:hep-ph/0509110].

[10] A. Birkedal, K. Matchev and M. Perelstein, Phys. Rev. Lett. **94** (2005) 191803 [arXiv:hep-ph/0412278].

[11] H. J. He *et al.*, Phys. Rev. D **78** (2008) 031701 [arXiv:0708.2588 [hep-ph]].

[12] A. Alves, O. J. P. Eboli, M. C. Gonzalez-Garcia and J. K. Mizukoshi, Phys. Rev. D **79** (2009) 035009 [arXiv:0810.1952 [hep-ph]].

[13] J. G. Bian *et al.*, Nucl. Phys. B **819** (2009) 201 [arXiv:0905.2336 [hep-ex]].

[14] T. Han, H. S. Liu, M. x. Luo, K. Wang and W. Wu, Phys. Rev. D **80** (2009) 095010 [arXiv:0908.2186 [hep-ph]].

[15] W. S. Cho, K. Choi, Y. G. Kim and C. B. Park, Phys. Rev. D **79** (2009) 031701 [arXiv:0810.4853 [hep-ph]].

[16] K. Choi, S. Choi, J. S. Lee and C. B. Park, Phys. Rev. D **80** (2009) 073010 [arXiv:0908.0079 [hep-ph]].

[17] K. Choi, J. S. Lee and C. B. Park, arXiv:1008.2690 [hep-ph].

[18] C. G. Lester and D. J. Summers, Phys. Lett. B **463** (1999) 99 [arXiv:hep-ph/9906349].

[19] R. S. Chivukula, B. Coleppa, S. Di Chiara, E. H. Simmons, H. J. He, M. Kurachi and M. Tanabashi, Phys. Rev. D **74** (2006) 075011 [arXiv:hep-ph/0607124].

[20] R. S. Chivukula, H. J. He, M. Kurachi, E. H. Simmons and M. Tanabashi, Phys. Rev. D **78** (2008) 095003 [arXiv:0808.1682 [hep-ph]].

[21] R. Casalbuoni, S. De Curtis, D. Dominici and R. Gatto, Phys. Lett. B **155** (1985) 95.

[22] R. Casalbuoni, A. Deandrea, S. De Curtis, D. Dominici, R. Gatto and M. Grazzini, Phys. Rev. D **53** (1996) 5201 [arXiv:hep-ph/9510431].

[23] T. Abe, S. Matsuzaki and M. Tanabashi, Phys. Rev. D **78** (2008) 055020 [arXiv:0807.2298 [hep-ph]].

[24] J. Alwall *et al.*, JHEP **0709** (2007) 028 [arXiv:0706.2334 [hep-ph]].

[25] N. D. Christensen *et al.*, arXiv:0906.2474 [hep-ph].

[26] T. Sjostrand, L. Lonnblad, S. Mrenna and P. Z. Skands, arXiv:hep-ph/0308153.

[27] M. L. Mangano, M. Moretti, F. Piccinini, R. Pittau and A. D. Polosa, JHEP **0307** (2003) 001 [arXiv:hep-ph/0206293].

[28] G. Corcella *et al.*, JHEP **0101** (2001) 010 [arXiv:hep-ph/0011363].

[29] G. Corcella *et al.*, arXiv:hep-ph/0210213.

[30] E. Richter-Was, arXiv:hep-ph/0207355.

[31] I. Hinchliffe, F. E. Paige, M. D. Shapiro, J. Soderqvist and W. Yao, Phys. Rev. D **55**, 5520 (1997) [arXiv:hep-ph/9610544].

[32] T. Ohl and C. Speckner, Phys. Rev. D **78** (2008) 095008 [arXiv:0809.0023 [hep-ph]].

[33] A. Alves, O. J. P. Eboli, D. Goncalves, M. C. Gonzalez-Garcia and J. K. Mizukoshi, Phys. Rev. D **80** (2009) 073011 [arXiv:0907.2915 [hep-ph]].

[34] F. Bach, Master theis, SPIRES entry